2026 IEEE/SICE International Symposium on System Integration (SII)
January 11-14, 2026. Cancún, México

Robotic Integration of Pneumatic Grasping Systems for Deformable Textile Handling: Automated Characterization Approach

Tristan Alkis[1], Ann Majewicz Fey[2], and Roman Mykhailyshyn[3]

***Abstract*— The integration of automated systems for the manipulation of deformable objects in manufacturing remains a time-consuming process. This challenge arises primarily from the absence of standardized grasping parameters applicable to the full range of manufactured products and materials. This paper presents a method for automating the study of the lifting parameters of deformable objects using a robotic manipulator with a pneumatic grasping system. A detailed description of the design, implementation, and evaluation of a custom pneumatic gripper integrated with a robot arm is provided. Through experiments utilizing various gripping surfaces and materials, the influence of surface patterns, material properties, and pneumatic pressures on lifting performance was investigated. The results demonstrate significant correlations between material type, surface design, and supply pressure in the context of gripping porous objects. The proposed method enables rapid characterization of the interaction between materials and pneumatic grasping systems. This approach facilitates the integration of pneumatic gripping systems into fully automated manufacturing lines handling deformable objects.**

I. Introduction

The grasping, lifting, and manipulation of deformable objects is an important part of both manufacturing and other automated operations in everyday human life [1], [2]. Textiles are the most used materials in everyday life and manufacturing. However, automation of textile material manipulation operations is very complex [3]–[8]. Although specialized areas of robotics focus on manipulating and grasping clothing using industrial robots [9]–[13], the problems with the speed of manipulation and the analysis of the deformations that accompany it remain a difficult issue [14], [15].

The grasping process is crucial to the issue of manipulating textile objects and their stability. Therefore, the development of gripping devices for deformable objects is a key direction for automating this process [16]–[21]. There are many different types of gripping devices that can be used to grip textiles. However, the most commonly used are mechanical and pneumatic grippers. When mechanical grippers are used with a small number of fingers [22]–[25], their control is simplified, but this does not allow for the effective gripping of thin objects. With an increase in the number of fingers, it is practically very difficult to achieve the accuracy of movements that would provide the required result [26], [27]. At the same time, pneumatic grippers are most often used in production due to the ease of control. When using pneumatic grippers with textile (porous) objects, a significant loss in the negative pressure created by the grippers is observed [17]. This leads to a loss of lifting force, which increases the energy costs of the entire transportation process. Therefore, many different types of combined (pneumatic with needle [23]) and unique designs (jet [18], electrostatic [22], rotary [16], etc.) are used.

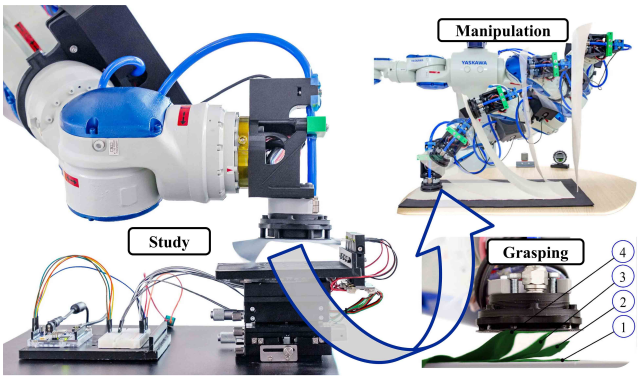

Fig. 1: Diagram different stages of studying the gripping process to provide the implementation of automated grasping [17], [18], [30], lifting [7], and manipulation of deformable objects [8] in manufacturing.

The development of new local jet gripping devices [17], [18], provides the opportunity to quickly grasp textile (porous) objects from a distance and at different orientations (Fig. 1). These local jet gripping devices are essentially modified Bernoulli gripping devices. There is a large amount of research focused on optimizing the shape [28]–[30] and manufacturing methods of these devices [31], which allows to automate the process of grasping and manipulating not only textile but also other deformable objects such as human tissues [32].

An analysis of the latest methods for manipulating deformable objects [8] reveals opportunities to effectively use even classic pneumatic devices for deformable objects (Fig. 1). It is also known from previous studies [7] that the greatest influence on the ability to grasp and manipulate deformable textile materials is their porosity. Textile materials have different porosity, which leads to depressurization of the gripper cavity and a decrease lifting force. These parameters in combination have not been studied in previous works, and to apply novel manipulation methods [8], it is necessary to

[1]Tristan Alkis is with the Department of Mechanical Engineering, The University of Texas at Austin, Austin, TX 78712, USA, and with the Prime Controls, LP, Lewisville, TX 75057, USA. tristan_alkis@utexas.edu

[2]Ann Majewicz Fey is with the Department of Mechanical Engineering, The University of Texas at Austin, Austin, TX 78712, USA. Ann.MajewiczFey@utexas.edu

[3]Roman Mykhailyshyn is with the National Institute of Advanced Industrial Science and Technology (AIST), Tokyo 135-0064, Japan, also with the EPAM School of Digital Technologies, American University Kyiv, Kyiv, 02000, Ukraine, and on leave from the Department of Mechanical Engineering, The University of Texas at Austin, Austin, TX 78712, USA. (Corresponding author e-mail: roman.mykhailyshyn@aist.go.jp)

know the parameters of the system (lifting force, coefficient of friction, etc.). This increases the time it takes to integrate such technologies in manufacturing. Therefore, this article aims to study the interaction process of pneumatic gripping devices with deformable objects and automate this process. To achieve this, an automatic system and an experiment algorithm were developed to determine the parameters of pneumatic gripping devices, such as lifting force and negative pressure in the gripper cavity. This paper demonstrates a study investigating the influence of the shape and size of the gripper grid on its parameters during interaction with textile materials.

II. Methodology

The process of studying deformable objects is very complex and depends on the goal and environment. When using classical mechanical methods of grasping [10], there are a large number of benchmarking [33]–[35] and taxonomies [36] to evaluate the interaction of a robot with a deformable object. Usually, they are reduced to finding the parameters of the object by stretching or compressing, and the parameters of the tasks for the robot, like: dragging, folding/unfolding, stacking/unstacking, spreading, and pick-and-place deformable objects. However, these methods do not obtain important system parameters from the point of view of using pneumatic grippers. Therefore, this section details the methods for determining the system parameters during the interaction of a pneumatic gripping system and deformable (porous) objects.

A. Setup

An experimental setup (Fig. 2) has been developed to determine the characteristics of the interaction between pneumatic gripping devices and deformable objects. The setup is based on an industrial robot SDA10F Yaskawa Dual Arm (repeatability ± 0.1 mm) to which a gripper control box is connected, and a pneumatic gripping device is connected to the end effector via an adapter. All adapters, fasteners, and elements of the gripping system are made by 3D printing from PLA filament. To control the gripper, several elements are used; the first is the air pressure control using a regulator with a digital sensor attached to the table. The second part of the compressed air supply control is the gripper control box, which consists of an Arduino controller, a relay, and a solenoid valve. After opening the valve, the compressed air flows to the vacuum generator (ejector Yimaida Model CV-15HS), which is attached to the end-effector adapter, and creates a negative pressure in the tube connected to the gripper chamber. Depending on the supply pressure and the sealing integrity of the pneumatic gripper, a negative pressure is created in the cavity and under the aerial gripper grid. To determine the resulting negative pressure in the cavity of the gripper, a pressure sensor -100 to 100 kPa (SMC ZSE20) is used.

The studied material is fixed to the force sensor (Zemic H3-C3-50kg-3B model load cell), which is attached to a table (or other stationary surface). The analog signal from the sensor is processed based on FB THOR Precision (Torbal

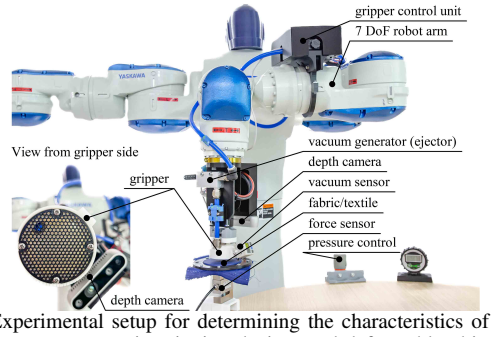

Fig. 2: Experimental setup for determining the characteristics of the interaction between pneumatic gripping devices and deformable objects.


(a) (b)
Fig. 3: Study textile materials: (a) - satin; (b) – 600 denier.


(a) (b)
Fig. 4: Studying active surfaces of aerial gripping device: (a) - with different infill densities (triangular shape): 30%, 40%, and 50%; (b) - with different surface shapes (30% infill): square, circle and star.

with an accuracy of $\pm 0.2\%$, 80 Hz), which is digitally transmitted to the workstation. The position and orientation of the object relative to the gripping device are localized using a depth camera. The Intel RealSense Depth Camera D435i is attached to the end-effector adapter to ensure the automated study of the interaction between pneumatic gripping devices and deformable objects. The Yaskawa arm was controlled through ROS using Python scripting, with initial MoveIt configuration from the ROS-Industrial Motoman repository on Github [37].

B. Variable Parameters

To demonstrate the influence of material parameters on the study, two fabrics with opposite parameters were used: satin and 600 denier Cordura outdoor canvas water-proof fabric[1], shown in Fig. 3a and Fig. 3b. As mentioned earlier, the greatest influence on the ability to grasp and manipulate deformable textile materials is porosity, so one of the most porous materials, satin, and the least porous, 600 denier, was chosen. The 600 denier is a coarse fabric on one side with a waterproofing composite on the other. The testing of the denier fabric was conducted on the side that is the coarse fabric. The satin is smooth and porous, allowing air to pass easily through.

In pneumatic aerial grippers (diameter 60 mm), one of the most important components is the grid, which limits the volume of air that can pass through and is the point of contact with the gripping surface. Therefore, the first parameter that plays a significant role when choosing a grid is its porosity (filling during 3D printing). Three varied options were tested: thirty percent infill, forty percent infill, and fifty percent infill for each gripping surface (Fig. 4a). Another non-obvious

[1]Available [Online]: https://romanmykhailyshyn.github.io/portfolio/portfolio-1/

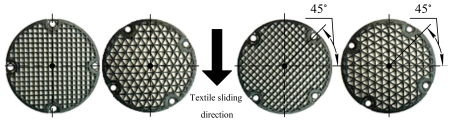

Fig. 5: Different orientations of gripper grids (square and triangle), left is 0 deg, and the right is 45 deg. The direction of sliding of the textile relative to the orientation of the gripper (grid) is indicated, respectively the gripper moves from bottom to top.

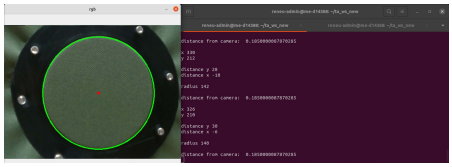

Fig. 6: Identifying the fabric location in terms of x, y, and z distance from the camera using the Hough Circle Transform.

parameter that is important when choosing a grid is the infill shape for 3D printing. When interacting with rigid objects, the grid infill shape will have almost no effect. Non-rigid objects will deform inside the grid and create additional friction forces [7]. Therefore, the second factor is the grid infill shape, and the following four shapes were investigated: square, triangle, circle, and star grid (Fig. 4b). To test the hypothesis that when a textile material is deformed inside the grid under the action of a suction force and the gripper starts to slide along the textile, depending on the orientation of the grid, an additional friction force may be created, which may lead to an increase in the holding force of the material. Therefore, this study investigated the effect of the grid orientation in relation to the direction of movement of the gripper (Fig. 5), 0 degrees left, 45 degrees right.

C. Testing Procedure

1) Coefficient of Friction Test: The coefficient of friction tests were conducted with triangle and square surfaces, as depicted in (Fig. 5). Tests were performed with ten repetitions for each fabric, orientation, and infill percentage. The tests were conducted by securing each fabric to a heavy, flat glass surface using clamps (a detailed description of the methodology is provided in [7]). The robotic arm was oriented so that the gripping surface was facing upward and parallel to the ground. The fabric, secured to the glass, was then placed at its center of gravity on the gripping surface. The robotic arm was slowly rotated, increasing the slip angle until the fabric began to slip. At this angle, the robot motors were shut off, and the angle β was recorded. The movement was scaled to 0.001 of the maximum velocity (m/s) and acceleration (m/s^2). Having found the average value of the angle of onset of slip $\bar{\beta}$, it is possible to analytically determine the coefficient of friction using the equation $f = tan(\bar{\beta})$.

2) Pure Lifting Test: Based on the operating range of the ejector, four different supply pressures were selected for the test: 100 kPa, 200 kPa, 300 kPa, and 400 kPa. Ten tests were conducted for each combination of surface, pressure, and fabric. Force and pressure data were recorded throughout testing.

The fabrics that were used for testing were attached to a

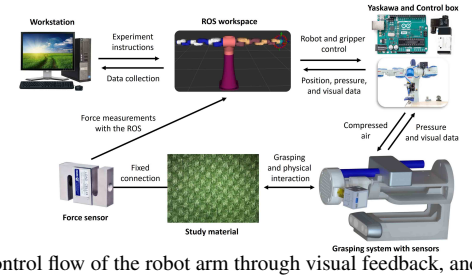

Fig. 7: Control flow of the robot arm through visual feedback, and collecting data from the end effector and force sensor.

round platform. The platform was identified through the use of the Intel RealSense camera and the Hough Circle Transfrom with OpenCV, as shown in Fig. 6. To improve platform identification while using the Hough Circle Transform, a color image was converted to grayscale and a Gaussian blur was implemented to smooth the edges. Parameters for the Hough Circle Transform and the Gaussian blur were optimized to find the best values for the depth and ranges of the experimental setup [38].

After identifying the platform using the Hough Circle Transform, the distance from the center of the gripping surface to the center of the fabric could then be calculated. To find the distance in the x-y plane, the center of the fabric was identified in pixel coordinates, the robot arm was then moved 4 mm in the x direction and 4 mm in the y direction, and new pixel coordinates for the center of the fabric were identified. The distance between the initial and final coordinates in pixels was determined using (1), and (2) was used to calculate the conversion from pixels to millimeters. Using (3) the rotation between the robot axis and the camera axis can be found and then aligned. The center of the fabric can then be identified and the robot arm can be moved the specified distance using (1) and (2).

$$D = \sqrt{(\Delta x)^2 + (\Delta y)^2}, \tag{1}$$

$$S = \frac{D_{\text{mm}}}{D_{\text{pixels}}}, \tag{2}$$

$$\theta = \tan^{-1}\left(\frac{\Delta y}{\Delta x}\right), \tag{3}$$

The depth reading from the camera to the fabric was then calculated because the camera was centered over the fabric. From this stage, the tool center point of the gripper was moved to the center of the platform.

Full contact with the deformable object and stability of the measurement results were ensured prior to recording force data from the sensor. The active surface of the gripper is pressed 1 mm in the direction of the object. After reaching the required position, the gripping device is turned on by supplying compressed air to the ejector. The robot arm stayed there for a second and then moved vertically 5 mm. The vertical movement was scaled to 0.001 mm/s of the robot's velocity and the minimum capable acceleration, to ensure collecting clear and high-quality data. Figure 7 depicts the control flow of the system, and Algorithm 1 outlines the algorithm described above for automating the lifting test.

3) Ninety-Degree Lifting Test: Based on previous studies of the force characteristics of pneumatic gripping devices [7],

Algorithm 1 Automated Process for Studying Lifting Force

Inputs: Configuration of the gripper to the study environment, infill percentage, configuration of the gripper-camera interface.
Output: Data collection from the force torque sensor, pressure measured inside the gripping chamber throughout testing.
Setup: The robot end effector is located so that the gripping surface is within the camera's field of view.

1: The camera attached to the end effector identifies the pixel coordinates of the center of the fabric using the Hough Transform as x_1 and y_1.
2: Move robot end effector 5 mm in robot X direction and 5 mm in robot Y direction.
3: Identify the pixel coordinates for the center of the fabric using the Hough Transform as x_2 and y_2.
4: Solve (1) numerically for pixel distance traveled.
5: Solve (2) numerically for the scale factor.
6: Using equation (3), solve for the angle between the camera axes and the robot's axes.
7: Using Hough Circle Transform and equations (1, 2) find the distance from the center of the camera to the center of the fabric.
8: The signs of the x and y distances from step 7 are flipped.
9: The robot is commanded to move the distance calculated from step 8.
10: Calculate the distance (z) from the camera to the center of the fabric.
11: The robot arm is commanded to move the gripping surface to the center of the fabric.
12: Force/torque data begins collection.
13: The script sends a signal to the Arduino, which then opens the solenoid valve.
14: The robot is commanded to lift the end effector 10 mm.
15: The Arduino closes the solenoid valve.
16: The robot is commanded to lower the end effector 10 mm.
17: Steps 13-16 are repeated nine more times.
18: The pressure within the gripping cavity is recorded throughout the testing.

Distance from the center of the camera to the center of the gripping surface is known. Orientation of the camera with pneumatic gripping surface is consistent across tests.

[17], [30], it can be stated that grid parameters have an impact on the gripper holding force, and this is especially observed when lifting deformable objects at an angle [7]. During grasping/holding, the deformable object sinks into the holes of the gripper grid, which increases the holding force due to the increase in the friction force. We ask ourselves the following question: *Does the shape and orientation of the grid elements affect the holding force*? Since the star and circle grid shapes are practically symmetrical, they were excluded from ninety-degree lifting tests, and the focus remained on the square and triangle shapes. For this testing, two different input pressures were used (200, 300 kPa), and ten repetitions were recorded for each fabric, orientation (as shown in Fig. 5), pressure, and infill percentage.

The test procedure begins with the robot arm oriented so that the plane of the gripping surface is perpendicular to the ground. The fabric was attached to a thin 3D printed structure to hold the fabric vertically. This structure was then attached to the force sensor that was held in place on the table by a clamp. Once the plane of the gripping surface was parallel to the plane of the fabric, and centered, the gripping surface was then pressed into the fabric. Next, a signal is sent to the controller, activating the solenoid valve to provide lifting force, and the robot arm is lifted by 10 mm. Then, the solenoid valve deactivates, the air supply is turned off, and the robot arm is retracted horizontally 10 mm. The arm is then lowered 10 mm and moved back 10 mm into the fabric. This process is repeated nine additional times. Data from the force sensor, as well as the pressure within the gripper cavity, were recorded throughout the experiment.

III. Results

It takes a lot of time and investment to integrate and evaluate the effectiveness of gripping technology and certain types of materials. Using the methodology proposed above (Section II), it is possible to automate the process of studying the interaction of pneumatic gripping devices with deformable objects in manufacturing. Providing an initial data analysis, we conducted a pure lifting test for two types of deformable materials: denier (Tab. I) and satin (Tab. II). Which is accompanied by changing the parameters: grid filling (30, 40, 50%), grid shape (square, triangle, star, circle), and supply pressure (100, 200, 300, 400 kPa). This allows us to find the lifting force of the pneumatic gripper and the negative pressure created in the gripper cavity.

After analyzing the data obtained (Tab. I, II) and their visualization (Fig. 8), we can see a realistic picture of the

TABLE I: Pure Lifting – Denier

%	Surface	100 kPa		200 kPa		300 kPa		400 kPa	
		F (N)	P (kPa)	F (N)	P (kPa)	F (N)	P (kPa)	F (N)	P (kPa)
30	Square	0.20 (0.00)	-16.6 (0.11)	0.42 (0.06)	-30.1 (0.06)	0.58 (0.06)	-41.1 (0.10)	1.04 (0.08)	-44.9 (0.08)
	Triangle	0.40 (0.00)	-15.2 (0.03)	0.60 (0.00)	-26.6 (0.06)	0.80 (0.06)	-31.1 (0.02)	0.82 (0.00)	-33.7 (0.05)
	Star	0.60 (0.13)	-12.0 (0.00)	0.74 (0.10)	-21.0 (0.00)	0.84 (0.08)	-26.0 (0.00)	0.86 (0.10)	-27.0 (0.00)
	Circle	0.60 (0.00)	-12.6 (0.05)	1.00 (0.10)	-21.3 (0.04)	1.05 (0.06)	-29.50 (0.02)	1.10 (0.00)	-30.0 (0.05)
40	Square	0.60 (0.00)	-18.6 (0.05)	0.82 (0.06)	-32.4 (0.05)	1.00 (0.00)	-40.1 (0.02)	1.00 (0.00)	-42.6 (0.11)
	Triangle	0.46 (0.10)	-21.5 (0.08)	0.78 (0.06)	-37.5 (0.05)	0.96 (0.08)	-48.6 (0.05)	0.96 (0.10)	-49.2 (0.03)
	Star	0.72 (0.14)	-16.0 (0.00)	0.92 (0.13)	-30.0 (0.00)	0.96 (0.10)	-37.0 (0.00)	1.04 (0.08)	-38.0 (0.00)
	Circle	0.62 (0.11)	-14.2 (0.04)	0.70 (0.06)	-26.8 (0.05)	0.80 (0.06)	-34.9 (0.03)	0.82 (0.00)	-35.0 (0.02)
50	Square	0.40 (0.00)	-10.0 (0.00)	0.58 (0.06)	-17.0 (0.00)	0.60 (0.00)	-20.1 (0.02)	0.60 (0.00)	-20.9 (0.02)
	Triangle	0.60 (0.00)	-21.9 (0.02)	0.80 (0.00)	-39.0 (0.06)	1.00 (0.00)	-50.0 (0.00)	1.00 (0.00)	-51.0 (0.00)
	Star	0.70 (0.14)	-22.0 (0.00)	0.82 (0.06)	-38.0 (0.00)	1.10 (0.17)	-49.0 (0.00)	1.12 (0.14)	-50.0 (0.00)
	Circle	0.40 (0.00)	-19.7 (0.04)	0.62 (0.06)	-32.4 (0.05)	0.80 (0.00)	-37.4 (0.04)	1.02 (0.20)	-39.0 (0.07)

All data is shown as mean (standard deviation). P is the pressure in the gripper cavity, F is the lifting force.

TABLE II: Pure Lifting – Satin

%	Surface	100 kPa		200 kPa		300 kPa		400 kPa	
		F (N)	P (kPa)	F (N)	P (kPa)	F (N)	P (kPa)	F (N)	P (kPa)
30	Square	0.44 (0.08)	-3.0 (0.00)	0.52 (0.10)	-4.0 (0.00)	0.62 (0.08)	-4.0 (0.00)	0.64 (0.06)	-4.0 (0.00)
	Triangle	0.24 (0.09)	-2.0 (0.00)	0.42 (0.11)	-4.0 (0.00)	0.52 (0.13)	-4.0 (0.00)	0.54 (0.14)	-4.0 (0.00)
	Star	0.42 (0.06)	-3.0 (0.00)	0.50 (0.14)	-4.0 (0.00)	0.50 (0.10)	-4.0 (0.00)	0.52 (0.14)	-4.0 (0.00)
	Circle	0.46 (0.10)	-3.0 (0.00)	0.62 (0.11)	-4.0 (0.00)	0.64 (0.10)	-4.4 (0.05)	0.66 (0.09)	-5.0 (0.00)
40	Square	0.42 (0.06)	-3.0 (0.00)	0.48 (0.14)	-4.0 (0.00)	0.64 (0.10)	-4.0 (0.00)	0.68 (0.08)	-4.0 (0.00)
	Triangle	0.44 (0.11)	-3.0 (0.00)	0.52 (0.09)	-4.0 (0.00)	0.52 (0.14)	-5.0 (0.00)	0.52 (0.14)	-5.0 (0.00)
	Star	0.44 (0.08)	-3.0 (0.00)	0.46 (0.97)	-4.0 (0.00)	0.52 (0.10)	-4.0 (0.00)	0.66 (0.14)	-4.0 (0.00)
	Circle	0.46 (0.10)	-3.0 (0.00)	0.52 (0.14)	-4.0 (0.00)	0.52 (0.14)	-5.0 (0.00)	0.54 (0.13)	-5.0 (0.00)
50	Square	0.34 (0.13)	-3.0 (0.00)	0.42 (0.11)	-4.0 (0.00)	0.44 (0.13)	-4.0 (0.00)	0.54 (0.09)	-4.0 (0.00)
	Triangle	0.28 (0.10)	-3.0 (0.00)	0.40 (0.13)	-4.0 (0.00)	0.52 (0.10)	-5.0 (0.00)	0.66 (0.11)	-5.0 (0.00)
	Star	0.46 (0.10)	-3.0 (0.00)	0.48 (0.10)	-4.0 (0.00)	0.66 (0.10)	-4.0 (0.00)	0.66 (0.10)	-4.0 (0.00)
	Circle	0.34 (0.13)	-3.0 (0.00)	0.48 (0.13)	-5.0 (0.00)	0.60 (0.10)	-5.0 (0.00)	0.60 (0.13)	-5.0 (0.00)

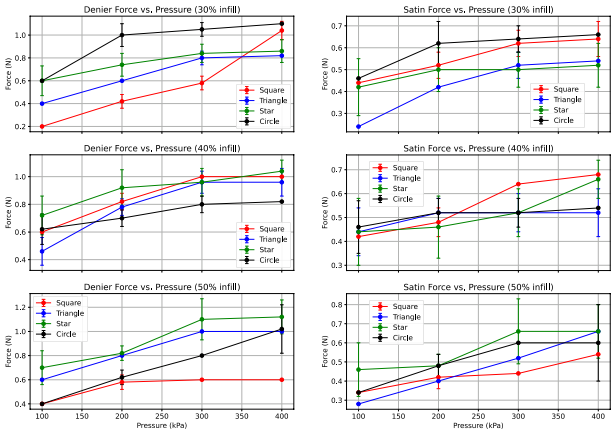

(a) (b)

Fig. 8: Comparison between lifting force and applied air pressure for: (a) denier; (b) satin.

increase in lifting force with increasing supply pressure for all combinations studied. This also applies to the decreased pressure in the gripper cavity as the supply pressure increases. Due to the presence of an impermeable coating on one side of the denier, the pneumatic gripping device creates a greater vacuum and provides a greater lifting force compared to satin. These parameters confirm the adequacy of the results obtained, with the standard deviation remaining very low on average, although errors of up to 30% are allowed for pneumatic systems. An important indicator is that the lifting force changes significantly when changing the type of grid and the percentage of filling. Since the mesh is made by 3D printing, this causes significant deviations in the indicators (porosity and, accordingly, lifting force) due to the influx of filament into the gaps of the grid. It is obvious that for both studied materials, the maximum lifting force is achieved when the grid is filled to 50%, and the maximum force is achieved when a star-type grid is used. It is also very noticeable that for the experiment with two materials, after reaching a supply pressure of 300 kPa, both the lifting force and the negative pressure in the gripper cavity practically do not change. In particular, for the denier, the lifting force increases on average by 10.8%, and the pressure in the gripper cavity decreases on average by 3.8% when comparing the data with supply pressures of 300 and 400 kPa. For satin, the lifting force increases on average by 8.4%, and the pressure in the gripper cavity decreases on average by 1.2% when comparing the data with supply pressures of 300 and 400 kPa. This trend shows that due to the design properties of the ejector, the pneumatic gripper cannot provide a decrease in the gripper chamber pressure even with an increase in the ejector supply pressure. This is caused by the porosity of the textile materials being gripped, and since the ejector has limitations in mass air flows, there is a limit to the negative pressure that such a system can provide. As a result, this allows us to optimally select the parameters of the gripping system for a specific type of material.

Data for ninety-degree lifting force and friction coefficients were obtained for denier (Tab. III) and satin (Tab. IV).

TABLE III: Ninety-Degree Lifting – Denier

%	Surface	200 kPa				300 kPa				Friction	
		0 deg.		45 deg.		0 deg.		45 deg.		0 deg.	45 deg.
		F (N)	P (kPa)	F (N)	P (kPa)	F (N)	P (kPa)	F (N)	P (kPa)	μ	μ
30	Square	1.08 (0.18)	-27.0 (0.00)	1.16 (0.22)	-27.0 (0.00)	1.40 (0.00)	-36.0 (0.00)	1.40 (0.00)	-36.0 (0.00)	0.272 (0.002)	0.274 (0.011)
	Triangle	1.00 (0.00)	-18.0 (0.00)	0.88 (0.11)	-18.0 (0.00)	1.04 (0.09)	-21.0 (0.00)	1.32 (0.18)	-21.0 (0.00)	0.268 (0.009)	0.274 (0.009)
40	Square	0.92 (0.27)	-26.0 (0.00)	0.88 (0.18)	-26.0 (0.00)	1.28 (0.11)	-33.0 (0.00)	1.16 (0.09)	-33.0 (0.00)	0.259 (0.005)	0.264 (0.008)
	Triangle	1.16 (0.22)	-26.0 (0.00)	1.16 (0.09)	-26.0 (0.00)	1.48 (0.18)	-32.8 (0.16)	1.52 (0.11)	-33.2 (0.11)	0.255 (0.004)	0.258 (0.005)
50	Square	0.60 (0.00)	-13.0 (0.00)	0.40 (0.00)	-13.0 (0.00)	0.84 (0.09)	-16.0 (0.00)	0.84 (0.09)	-16.0 (0.00)	0.266 (0.008)	0.262 (0.008)
	Triangle	1.16 (0.09)	-26.0 (0.00)	1.32 (0.11)	-28.0 (0.00)	1.53 (0.10)	-36.0 (0.00)	1.64 (0.22)	-36.0 (0.00)	0.255 (0.008)	0.251 (0.001)

TABLE IV: Ninety-Degree Lifting – Satin

%	Surface	200 kPa				300 kPa				Friction	
		0 deg.		45 deg.		0 deg.		45 deg.		0 deg.	45 deg.
		F (N)	P (kPa)	F (N)	P (kPa)	F (N)	P (kPa)	F (N)	P (kPa)	μ	μ
30	Square	0.12 (0.10)	-0.30 (0.00)	0.20 (0.00)	-3.0 (0.00)	0.20 (0.00)	-3.0 (0.00)	0.20 (0.00)	-3.0 (0.00)	0.360 (0.023)	0.360 (0.008)
	Triangle	0.20 (0.00)	-3.0 (0.00)	0.20 (0.00)	-3.0 (0.00)	0.20 (0.00)	-3.0 (0.00)	0.20 (0.00)	-3.0 (0.00)	0.313 (0.007)	0.313 (0.009)
40	Square	0.04 (0.09)	-3.0 (0.00)	0.04 (0.09)	-3.0 (0.00)	0.20 (0.00)	-3.0 (0.00)	0.20 (0.00)	-3.0 (0.00)	0.315 (0.007)	0.315 (0.006)
	Triangle	0.00 (0.00)	-3.0 (0.00)	0.20 (0.00)	-3.0 (0.00)	0.20 (0.00)	-3.0 (0.00)	0.20 (0.00)	-3.0 (0.00)	0.306 (0.007)	0.302 (0.005)
50	Square	0.20 (0.00)	-2.0 (0.00)	0.20 (0.00)	-2.0 (0.00)	0.20 (0.00)	-3.0 (0.00)	0.20 (0.00)	-3.0 (0.00)	0.338 (0.004)	0.296 (0.012)
	Triangle	0.20 (0.00)	-3.0 (0.00)	0.20 (0.00)	-3.0 (0.00)	0.20 (0.00)	-3.0 (0.00)	0.20 (0.00)	-3.0 (0.00)	0.296 (0.009)	0.277 (0.005)

This is accompanied by changing the parameters: grid filling (30, 40, 50%), grid shape (square, triangle), grid orientation (0 deg., 45 deg.), and supply pressure (200, 300 kPa). Comparing the pure and ninety-degree lifting experiments for denier, there is an average decrease in negative pressure in the gripper chamber of 23.8% and an average increase in the lifting force of 64.1% for a supply pressure of 300 kPa. The change in negative pressure in the gripper chamber negatively affects the lifting force, but due to the additional friction force there is an increase in the holding force. Comparing the pure and ninety-degree lifting experiments for satin, an average decrease in negative pressure in the gripper chamber of 30% and an average decrease in lifting force of 62.6% was observed for a supply pressure of 300 kPa. This negative effect is due to the low mass flow of the ejector, which does not allow the maintenance of negative pressure in the gripper cavity, reducing the real friction force attributed to the low contact with the material. The results obtained indicate the effectiveness of using the aerial pneumatic gripper for denier material and the ineffectiveness of using it for satin. Therefore, for more porous materials, it is worth using pneumatic gripping devices with a higher mass flow rate, for example, a textile gripper based on the Bernoulli or Coanda effects.

IV. Conclusion

The use and integration of pneumatic grippers in manufacturing is becoming increasingly widespread due to their efficiency, adaptability to various objects, and ease of control

compared to other types of grippers. This paper presented a method for automating the study of force characteristics essential to designing and integrating automated lines that interact with deformable objects. Using the proposed methodology, the interaction between an aerial pneumatic gripper and two deformable textile materials was investigated. The results revealed that effective gripping parameters were identified for manipulating the denier material, whereas the gripper configuration proved to be ineffective for satin. It was also observed that, for the studied materials and across all supply pressures, a gripping surface with a higher percentage of infill pattern gets better performance. The proposed method enables the creation of a dataset for all materials used in production, facilitating the identification of optimal pneumatic gripper parameters.

REFERENCES

[1] H. Yin, A. Varava, and D. Kragic, "Modeling, learning, perception, and control methods for deformable object manipulation," *Science Robotics*, vol. 6, no. 54, p. eabd8803, 2021.

[2] D. Henrich and H. Wörn, *Robot manipulation of deformable objects*. Springer Science & Business Media, 2012.

[3] D. Berenson, "Manipulation of deformable objects without modeling and simulating deformation," in *2013 IEEE/RSJ International Conference on Intelligent Robots and Systems*. IEEE, 2013, pp. 4525–4532.

[4] J. Sanchez, J.-A. Corrales, B.-C. Bouzgarrou, and Y. Mezouar, "Robotic manipulation and sensing of deformable objects in domestic and industrial applications: a survey," *The International Journal of Robotics Research*, vol. 37, no. 7, pp. 688–716, 2018.

[5] A. M. Howard and G. A. Bekey, "Intelligent learning for deformable object manipulation," *Autonomous Robots*, vol. 9, pp. 51–58, 2000.

[6] D. McConachie, A. Dobson, M. Ruan, and D. Berenson, "Manipulating deformable objects by interleaving prediction, planning, and control," *The International Journal of Robotics Research*, vol. 39, no. 8, pp. 957–982, 2020.

[7] R. Mykhailyshyn, A. M. Fey, and J. Xiao, "Toward novel grasping of nonrigid materials through robotic end-effector reorientation," *IEEE/ASME Transactions on Mechatronics*, vol. 29, no. 4, pp. 2614–2624, 2024.

[8] R. Mykhailyshyn, J. Lee, M. Mykhailyshyn, K. Harada, and A. M. Fey, "Dexterous manipulation of deformable objects via pneumatic gripping: Lifting by one end," *arXiv preprint arXiv:2501.05198*, 2025.

[9] D. Kruse, R. J. Radke, and J. T. Wen, "Collaborative human-robot manipulation of highly deformable materials," in *2015 IEEE international conference on robotics and automation (ICRA)*. IEEE, 2015, pp. 3782–3787.

[10] J. Borras, G. Alenya, and C. Torras, "A grasping-centered analysis for cloth manipulation," *IEEE Transactions on Robotics*, vol. 36, no. 3, pp. 924–936, 2020.

[11] I. Cuiral-Zueco and G. López-Nicolás, "Taxonomy of deformable object shape control," *IEEE Robotics and Automation Letters*, 2024.

[12] F. Coltraro, J. Borràs, M. Alberich-Carramiñana, and C. Torras, "Tracking cloth deformation: A novel dataset for closing the sim-to-real gap for robotic cloth manipulation learning," *The International Journal of Robotics Research*, p. 02783649251317617, 2025.

[13] A. Longhini, Y. Wang, I. Garcia-Camacho, D. Blanco-Mulero, M. Moletta, M. Welle, G. Alenyà, H. Yin, Z. Erickson, D. Held, *et al.*, "Unfolding the literature: A review of robotic cloth manipulation," *Annual Review of Control, Robotics, and Autonomous Systems*, vol. 8, 2024.

[14] J. Zhu, A. Cherubini, C. Dune, D. Navarro-Alarcon, F. Alambeigi, D. Berenson, F. Ficuciello, K. Harada, J. Kober, X. Li, *et al.*, "Challenges and outlook in robotic manipulation of deformable objects," *IEEE Robotics & Automation Magazine*, vol. 29, no. 3, pp. 67–77, 2022.

[15] R. Herguedas, G. López-Nicolás, R. Aragüés, and C. Sagüés, "Survey on multi-robot manipulation of deformable objects," in *2019 24th IEEE International Conference on Emerging Technologies and Factory Automation (ETFA)*. IEEE, 2019, pp. 977–984.

[16] J. Unde, J. Colan, and Y. Hasegawa, "Design, modelling, and experimental verification of passively adaptable roller gripper for separating stacked fabric," *IEEE Robotics and Automation Letters*, 2024.

[17] R. Mykhailyshyn, A. M. Fey, and J. Xiao, "Finite element modeling of grasping porous materials in robotics cells," *Robotica*, vol. 41, no. 11, pp. 3485–3500, 2023.

[18] R. Mykhailyshyn, V. Savkiv, A. M. Fey, and J. Xiao, "Gripping device for textile materials," *IEEE Transactions on Automation Science and Engineering*, vol. 20, no. 4, pp. 2397–2408, 2023.

[19] L. Birglen and T. Schlicht, "A statistical review of industrial robotic grippers," *Robotics and Computer-Integrated Manufacturing*, vol. 49, pp. 88–97, 2018.

[20] G. Fantoni, M. Santochi, G. Dini, K. Tracht, B. Scholz-Reiter, J. Fleischer, T. K. Lien, G. Seliger, G. Reinhart, J. Franke, *et al.*, "Grasping devices and methods in automated production processes," *CIRP annals*, vol. 63, no. 2, pp. 679–701, 2014.

[21] R. Mykhailyshyn, V. Savkiv, P. Maruschak, and J. Xiao, "A systematic review on pneumatic gripping devices for industrial robots," *Transport*, vol. 37, no. 3, pp. 201–231, 2022.

[22] S. Donaire, J. Borras, G. Alenya, and C. Torras, "A versatile gripper for cloth manipulation," *IEEE Robotics and Automation Letters*, vol. 5, no. 4, pp. 6520–6527, 2020.

[23] Y. Ebraheem, E. Drean, and D. C. Adolphe, "Universal gripper for fabrics–design, validation and integration," *International Journal of Clothing Science and Technology*, vol. 33, no. 4, pp. 643–663, 2021.

[24] D. Hinwood, D. Herath, and R. Goecke, "Towards the design of a human-inspired gripper for textile manipulation," in *2020 IEEE 16th International Conference on Automation Science and Engineering (CASE)*. IEEE, 2020, pp. 913–920.

[25] F. Von Drigalski, D. Yoshioka, W. Yamazaki, S.-G. Cho, M. Gall, P. M. U. Eljuri, V. Hoerig, M. Ding, J. Takamatsu, T. Ogasawara, *et al.*, "Naist openhand m2s: A versatile two-finger gripper adapted for pulling and tucking textile," in *2017 first IEEE international conference on robotic computing (IRC)*. IEEE, 2017, pp. 117–122.

[26] I. Huang, Y. Narang, C. Eppner, B. Sundaralingam, M. Macklin, R. Bajcsy, T. Hermans, and D. Fox, "Defgraspsim: Physics-based simulation of grasp outcomes for 3d deformable objects," *IEEE Robotics and Automation Letters*, vol. 7, no. 3, pp. 6274–6281, 2022.

[27] P. Song, J. A. C. Ramón, and Y. Mezouar, "Dynamic evaluation of deformable object grasping," *IEEE Robotics and Automation Letters*, vol. 7, no. 2, pp. 4392–4399, 2022.

[28] R. Mykhailyshyn, F. Duchoň, I. Virgala, P. J. Sinčák, and A. Majewicz Fey, "Optimization of outer diameter bernoulli gripper with cylindrical nozzle," *Machines*, vol. 11, no. 6, p. 667, 2023.

[29] R. Mykhailyshyn and J. Xiao, "Influence of inlet parameters on power characteristics of bernoulli gripping devices for industrial robots," *Applied Sciences*, vol. 12, no. 14, p. 7074, 2022.

[30] R. Mykhailyshyn, J. Romancik, K. Harada, and A. Majewicz Fey, "Vibration vanquished: Enhancing grasping of deformable objects with jet gripper technology," in *2025 IEEE 21st International Conference on Automation Science and Engineering (CASE)*. IEEE, 2025, pp. 2874–2880.

[31] R. Mykhailyshyn, F. Duchoň, M. Mykhailyshyn, and A. Majewicz Fey, "Three-dimensional printing of cylindrical nozzle elements of bernoulli gripping devices for industrial robots," *Robotics*, vol. 11, no. 6, p. 140, 2022.

[32] R. Mykhailyshyn and A. M. Fey, "Low-contact grasping of soft tissue using a novel vortex gripper," in *2024 International Symposium on Medical Robotics (ISMR)*, 2024, pp. 1–6.

[33] I. Garcia-Camacho, J. Borràs, B. Calli, A. Norton, and G. Alenyà, "Household cloth object set: Fostering benchmarking in deformable object manipulation," *IEEE Robotics and Automation Letters*, vol. 7, no. 3, pp. 5866–5873, 2022.

[34] A. B. Clark, L. Cramphorn-Neal, M. Rachowiecki, and A. Gregg-Smith, "Household clothing set and benchmarks for characterising end-effector cloth manipulation," in *2023 IEEE International Conference on Robotics and Automation (ICRA)*. IEEE, 2023, pp. 9211–9217.

[35] D. Blanco-Mulero, O. Barbany, G. Alcan, A. Colomé, C. Torras, and V. Kyrki, "Benchmarking the sim-to-real gap in cloth manipulation," *IEEE Robotics and Automation Letters*, vol. 9, no. 3, pp. 2981–2988, 2024.

[36] A. Longhini, M. C. Welle, I. Mitsioni, and D. Kragic, "Textile taxonomy and classification using pulling and twisting," in *2021 IEEE/RSJ International Conference on Intelligent Robots and Systems (IROS)*. IEEE, 2021, pp. 7564–7571.

[37] R.-I. Consortium, "Ros-industrial motoman support," 2024. [Online]. Available: https://github.com/ros-industrial/motoman

[38] G. Bradski, "The opencv library," 2000. [Online]. Available: https://opencv.org/